IOP PUBLISHING JOURNAL OF PHYSICS: CONDENSED MATTER

J. Phys.: Condens. Matter **20** (2008) 055219 (10pp) doi:10.1088/0953-8984/20/5/055219

Modulation of interlayer exchange coupling by ion irradiation in magnetic tunnel junctions

E Snoeck[1], P Baules[1], G BenAssayag[1], C Tiusan[2], F Greullet[2], M Hehn[2] and A Schuhl[3]

[1] CEMES-CNRS, Groupe NanoMatériaux, 29 rue Jeanne Marvig, BP 4347, 31055 Toulouse, France

[2] Laboratoire de Physique des Matériaux, UMR CNRS 7556, Université de Nancy, Boulevard des Aiguillettes, BP 239, 54506 Vandoeuvre-lès-Nancy Cedex, France

[3] Laboratoire SPINTEC, URA 2512, Avenue des Martyrs, 38054 Grenoble, France

Received 4 September 2007, in final form 17 December 2007
Published 18 January 2008
Online at stacks.iop.org/JPhysCM/20/055219

Abstract

Ion implantation of epitaxial Fe/MgO/Fe magnetic tunnel junctions exhibiting antiferromagnetic exchange coupling by spin polarized tunneling has been performed. X-ray reflectivity and transmission electron microscopy experiments were performed to extensively study the structural changes of the junctions. Electron holography and vibrating sample magnetometry experiments show that the amplitude and the nature of the coupling are modified by the irradiation. A gradual increase in the bilinear and the biquadratic coupling has been measured when the ion dose increases. For large doses, the net coupling becomes ferromagnetic. This corresponds to an intermixing of the MgO barrier with the adjacent Fe layers which is demonstrated by x-ray reflectivity.

(Some figures in this article are in colour only in the electronic version)

1. Introduction

Antiferromagnetic (AF) coupling between two ferromagnetic (F) layers separated by a thin insulating barrier has been evidenced by Faure-Vincent *et al* [1] in Fe/MgO/Fe/MgO(001) epitaxial magnetic tunnel junctions (MTJs). This coupling was associated with the quantum tunneling of spin polarized electrons. The authors have demonstrated a transition from AF to F coupling for a MgO spacer thicker than 1 nm. This transition is due to the competition between (i) interlayer exchange coupling (IEC) by tunneling which favors anti-parallel (AP) alignment of both ferromagnetic layers at very small MgO thicknesses, and (ii) roughness induced magnetostatic orange-peel coupling favoring parallel (P) alignment. The experimental evidence for AF coupling supports the theoretical model proposed by Slonczewski [2] of an interlayer exchange due to spin polarized quantum tunneling of electrons between the two Fe layers. However, the free electron like model of Slonczewski does not take into account all the specific aspects of the spin polarized tunneling in epitaxial systems, i.e. the equilibrium propagation of different symmetry states for each spin channel, in each configuration of magnetizations [3]. Recently, similar results on magnetic coupling by spin polarized tunneling have been reported by Katayama *et al* [4]. In their systems, the sign and the origin of the AF coupling has been correlated with the oxygen vacancies in the MgO barriers. This interpretation is in agreement with the resonant tunneling models recently developed by Zhuravlev *et al* [5]. In these models, the authors argue the existence of an additional resonant tunneling mechanism in order to explain the sign of the coupling observed in the Fe/MgO/Fe junctions. However, in our epitaxial Fe/MgO/Fe systems we found no evidence of oxygen vacancies in the MgO barriers. Nevertheless, even if one neglects any impurity-associated level within the MgO barrier, a resonant level naturally exists at the Fe/MgO interface. Indeed, the interfacial minority resonance of Fe(001) provides the resonant equilibrium tunneling mechanism, as shown in the *ab initio* calculations of Wunnicke *et al* [6]. The equilibrium tunnel transport in the AP configuration is dominated by the propagation of the interfacial resonance (related to the surface state of Fe(001)). We reproduced the scanning tunneling

microscopy (STM) experiments of Bischoff *et al* [7] for our Fe(100) samples and clearly identified the Fe(001) surface state. It has a d_{z2} orbital character belonging to the Δ_1 symmetry and is located in the minority spin channel [3]. Theoretical calculations [3] have shown that the interfacial resonance of Fe is preserved at the Fe(100)/MgO interface. Hence, we argue that the resonant propagation of the interfacial resonance could be the main origin for the AF coupling observed in our Fe/MgO/Fe junctions. Moreover, our STM experiments show that the surface state of Fe is extremely sensitive to the roughness. Therefore, one expects a strong decrease of the IEC when the interfacial resonance is quenched by the roughness [7]. The most critical parameters for the coupling strength in a Fe/MgO/Fe system are then the MgO barrier thickness (the coupling by tunneling is extremely sensitive to the insulator thickness) and the quality of the top and bottom Fe/MgO interfaces (interfacial roughness destroys the interfacial resonance of Fe(001)). In our previous paper [1], we investigated the variation of the coupling strength as a function of the MgO thickness. After a rapid decay in the low MgO thickness range (0.6–0.8 nm) the sign of the coupling changes and becomes ferromagnetic. This corresponds to the critical thickness beyond which the growth of the MgO barrier on Fe(001) stops being pseudomorphic as proven by reflection high energy electron diffraction (RHEED) intensity oscillations [1]. Misfit dislocations then appear in the MgO layer leading to a greater roughness of the top MgO/Fe interface. This roughness induces orange-peel F coupling which overcomes the AF one. As a result, a net F coupling emerges for an MgO spacer above 0.8 nm thick.

In this paper we propose a different way to modulate the IEC strength. For a fixed MgO barrier thickness we modify the Fe/MgO interface roughness in order to study in more detail the influence of the interfacial microstructure on the IEC. For that purpose, we irradiated epitaxial Au/Pd/Fe/MgO/Fe/MgO(001) MTJs with N^+ ions at 150 keV. The ion irradiation simulations indicate that most of the deposited energy is located at the top Au/Pd, Pd/Fe and Fe/MgO interfaces. The most interesting for tuning the IEC coupling nature and strength is control of the quality of the Fe/MgO interface by adjusting the irradiation dose. The modification of the MTJ interfacial structure/morphology as a function of the irradiation dose has been investigated by x-ray reflectivity (XRR) and transmission electron microscopy (TEM), while their magnetic behavior has been studied by vibrating sample magnetometry (VSM) (macroscopic level) and electron holography (EH) (microscopic level).

Within this paper, we demonstrate that the roughness induced by the irradiation at the Fe/MgO interface destroys the AF coupling. Two mechanisms may contribute to the change of the coupling from AF to F. Bischoff *et al* [7] have shown by scanning tunneling spectroscopy (STS) experiments on Fe(001) surfaces that the roughness destroys the Fe(001) interfacial resonance state (IRS). If we assume that the AF coupling is strongly correlated to the resonant propagation across the barrier of the Fe(001) IRS [6], one then expects a decrease of the AF coupling strength when the roughness increases. Moreover, if the sign of the AF coupling is determined by a resonant tunneling mechanism [5], we then anticipate a reversal of the coupling (from AF to F) when the Fe(001) IRS is destroyed by the roughness. Moreover, for large Fe/MgO roughness direct ferromagnetic coupling may occur across the barrier. In our Fe/MgO/Fe system with an extremely thin insulating spacer (three MgO atomic planes), ferromagnetic bridges may locally appear across the MgO spacer. The TEM analyses performed on irradiated samples do not evidence clear metallic Fe 'bridges' (pinholes) within the MgO barrier while x-ray reflectivity indicates an increase of the barrier density with the dose. Then we assume that the ferromagnetic bridges may be represented by local regions with increased density of Fe atoms that have diffused within the MgO. The holography analyses demonstrate that these highly Fe doped regions in the MgO barrier provide a direct ferromagnetic interaction. The density of these ferromagnetic bridges increases with the irradiation dose and, for large doses, the ferromagnetic coupling becomes dominant. However, it remains difficult to experimentally uncorrelate the two mechanisms which affect the coupling strength and sign, i.e. (i) the quenching of the IRS by roughness and (ii) the occurrence of ferromagnetic bridges. The STS experiments studying the influence of roughness on the Fe surface state located in the minority spin band are only performed on free Fe(001) surfaces. Nevertheless, theoretical calculations [3] show that this surface state is preserved in the Fe/MgO/Fe(001) system, and becomes an interfacial resonant state (IRS). We then assume that the roughness induced quenching measured by STM can be correlated with the roughness induced quenching of the IRS in a full Fe/MgO/Fe stack. Moreover, the holography experiments provide information about the sign of the local coupling in a Fe/MgO/Fe tri-layer. This is correlated with the data obtained from complementary structural studies of the stacking (XRR and TEM). We then can extrapolate and argue on the influence of roughness on the resonant propagation of tunneling electrons in a Fe(001)/MgO/Fe system and therefore on the coupling strength and sign.

2. Experiment

2.1. Epitaxial growth of the MTJs

The MTJs were grown in a molecular beam epitaxy system on MgO(100) substrates, flashed at 600 °C before the growth of the layers. A 10 nm thick MgO layer is deposited on the substrate at 450 °C to decrease the roughness and trap the residual carbon impurities [8]. The base pressure in the UHV chamber before the deposition was 4×10^{-11} mbar. The Fe films were deposited from a Knudsen cell containing bulk Fe heated to 1280 °C. The bottom 30 nm thick Fe electrode was deposited at room temperature then annealed at 450 °C for 25 min to achieve a high crystalline quality. The 0.6 nm thick MgO insulating barrier is evaporated at 100 °C on the Fe surface by means of an electron gun. Within the thickness range of the samples investigated here, the two-dimensional layer-by-layer growth was assisted by RHEED intensity oscillations which enable an extremely precise control of the barrier thickness (three atomic planes).

On the MgO barrier, a second top 10 nm thick Fe electrode was grown at 100 °C. Finally, a Pd (10 nm)/Au (7 nm) capping bilayer has been deposited to prevent the *ex situ* oxidation of the top Fe layer. The growth of the different layers was *in situ* controlled by RHEED. Additional details concerning the epitaxial growth conditions of the samples have been reported in [9] and references therein.

2.2. Ion implantation

A Varian 200A2 ion implanter was used for N^+ irradiation. The ion beam is normal to the sample surface with an incident energy of 150 keV. Multilayers were irradiated at room temperature in a dose range from 10^{13} to 3×10^{16} ions cm^{-2}. The N^+ ions were chosen because of their chemical neutrality. A small ionic current, lower than 25 μA, was chosen to protect samples from heating and annealing effects. Prior to implantation, IPROS simulations, which are based on Monte Carlo collisional ion stopping computations, were performed [10]. They predict nearly light ion behavior for N^+ at 150 keV, which induces very short-range displacements for target atoms and nearly no implanted impurities in the layers of interest (Au, Pd, Fe and MgO): the ions pass through the multilayer and stop below in the MgO substrate.

2.3. X-ray reflectivity (XRR)

A Seifert θ–2θ x-ray diffractometer fitted with a double monochromator using Cu Kα radiation was used for x-ray reflectivity measurements. The experimental reflectivity profiles were simulated using two pieces of softwares: the home made 'Simurx'[4] and 'SimuReflec' [11] to measure the mean thicknesses and densities of the different layers and the interface roughness. Both simulation programs give similar values of roughness and thickness with an error bar of about ± 0.1 nm.

2.4. Transmission electron microscopy (TEM) studies

The cross-sectional specimens for TEM studies were cut along (100) MgO planes, glued face to face then thinned by mechanical grinding and ion-milling to the electron transparency. The structures of the different layers and interfaces were investigated by TEM both in conventional and in high resolution mode (HRTEM) using a FEI-F20 microscope fitted with a spherical aberration (Cs) corrector (CEOS) whose point resolution is 0.13 nm. We used off-axis electron holography in the same microscope to study the remanent magnetic state of the two Fe layers at room temperature and locally study the IEC. Holograms were digitally acquired with the conventional objective lens switched off and using the first transfer lens of the Cs corrector to reach a maximum magnification of 43 000× [12]. Electron holography allows recording of the amplitude and the phase shift of a high energy electron wave that has passed through a material [13]. The phase shift is sensitive to electrostatic [14, 15] and magnetic [16, 17] fields in the sample, and is given by the expression

$$\phi(x) = C_{\mathrm{E}} \int V_0(x, z)\,\mathrm{d}z - \frac{e}{\hbar} \int\int B_{\perp}(x, z)\,\mathrm{d}x\,\mathrm{d}z \quad (1)$$

where x is a direction in the plane of the sample, z is the incident electron beam direction, C_{E} is a constant that takes a value of 7.26×10^6 rad V^{-1} m^{-1} at a microscope accelerating voltage of 200 kV, V_0 is the electrostatic potential and $B_{\perp}$ is the component of the magnetic induction (both inside the sample and in the surrounding leakage fields) perpendicular to both x and z. Reference holograms were systematically acquired to remove distortions associated with the imaging and recording systems. For the MTJs studied here, the electrostatic contribution to the phase shift is associated solely with the mean inner potential (MIP), V_i, which depends on the local composition and density of the sample [18]. The magnetic contribution to the phase shift was obtained by recording two holograms between which the MTJs were magnetized parallel and then anti-parallel to their length. This is achieved by tilting the sample by $\pm 45°$ about an axis parallel to the stacking direction and switching the microscope objective lens on fully to apply a large in-plane field of about 13 kOe to the sample [19]. The objective lens was then switched off and the sample tilted back to zero to record each hologram. This procedure relies on the ability to saturate the magnetization in the sample in exactly two opposite directions (i.e. along the Fe layers) before decreasing the magnetic field back to the remanent state. This is a good condition, since the sample preparation of the MTJs for TEM experiments creates important shape anisotropy along the Fe layers. According to equation (1), half of the sum and half of the difference of the phase images obtained with the sample magnetized in opposite directions provide the electrostatic and magnetic contributions to the phase, respectively. Contours formed from the magnetic contribution to the phase provide an immediate visual picture of the magnetic field in the sample. The spacing of these contours is inversely proportional to the in-plane component of the magnetic induction in the sample integrated in the incident electron beam direction. Assuming a constant magnetization within the layers of thickness t in the direction of the beam, the magnetic contribution to the phase is

$$\phi_{\mathrm{Mag}}(x) = \frac{e \cdot t}{\hbar} \int B_{\perp}(x)\,\mathrm{d}x, \quad (2)$$

whereas the electrostatic contribution to the phase is

$$\phi_{\mathrm{Elec}}(x) = C_{\mathrm{E}} V_i \cdot t. \quad (3)$$

Note that for material whose MIP (V_i) is known ϕ_{Elec} gives access to the measurement of the thickness (t) of the TEM sample.

2.5. Magnetic experiments

Magnetic measurements were performed at two complementary different scales. The characterization of magnetism at a nanometric scale was done using the holography technique described in detail in the section dedicated to TEM studies. The

[4] The simulation software 'Simurx' can be freely downloaded. Requests must be addressed to Dr P Baules. E-mail: baules@cemes.fr

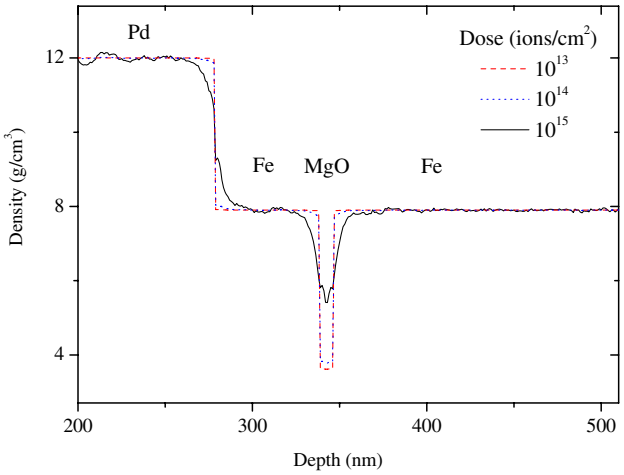

Figure 1. Simulation of the density changes in the Au/Pd/Fe/MgO/Fe stacking as a function of the ion dose (10^{13}, 10^{14}, and 10^{15} ions cm^{-2}).

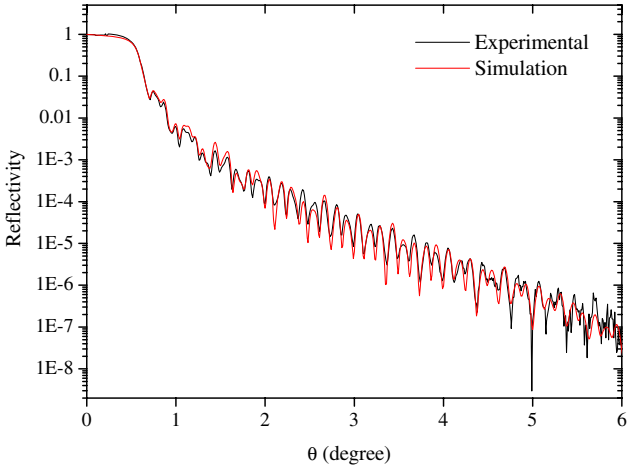

Figure 2. Experimental and simulated XRR spectra obtained on the as-deposited MTJ.

samples were magnetically characterized macroscopically, by VSM experiments, at room temperature. The VSM measurements were performed on continuous film samples with an in-plane applied magnetic field of ±0.8 kOe.

3. Ion implantation modeling

The ballistic effect of the ion implantation is simulated using IPROS which is a home made Monte Carlo ion implantation and collision code [10]. This code allows modeling of the complete stacking of different layers and calculating the effect of the ion implantation on the mixing of these layers. The calculations were done using the true layer stacking sequence measured by TEM (see below). We calculated the profile of the distribution of the recoil atoms of each type of species present in the different layers after ion implantation. These curves permit us to deduce the local composition of the different layers as a function of the doses but without taking into account the possible diffusion of the atoms due to the temperature during the implantation process. The plots in figure 1 show the different density profiles as a function of depth for doses of 10^{13}, 10^{14} and 10^{15} ions cm^{-2}. For higher doses the simulations with IPROS become less reliable and a code such as TRIDYN should be used to take into account the variation of the target stoichiometry with the implantation [20, 21]. Nevertheless for moderate doses the calculations performed using IPROS or SRIM are quite similar. These simulations indicate that the implantation induces an intermixing, especially in the top Fe layer and in the barrier. The local concentration of Fe increases in the MgO layer for a dose higher than 10^{14} ions cm^{-2}. These calculations also show that the Pd/Fe interface becomes more and more diffuse and that the top Fe layer is contaminated by Pd atoms.

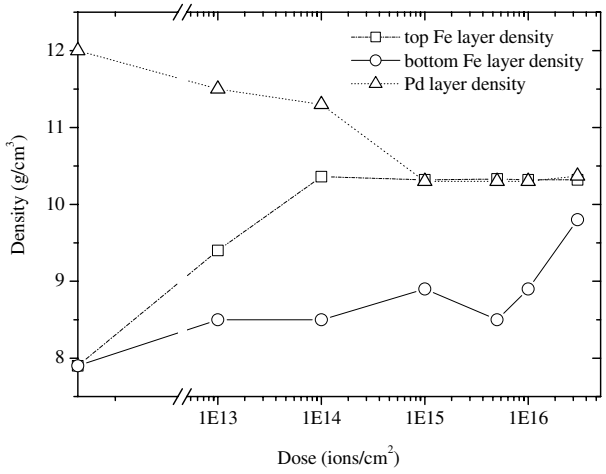

Figure 3. Changes in the densities of the Pd, top Fe and bottom Fe layers as a function of the ion dose (the points on the left axis represent the densities of the as-deposited layers).

4. Structural studies

4.1. X-ray reflectivity

X-ray reflectivity measurements were performed to study the mean changes of the irradiated MTJs as a function of the ion dose. An XRR spectrum obtained on the as-deposited MTJs is plotted in figure 2 together with its corresponding fit. The simulation of such a spectrum allows the mean microstructure of the stacking to be recovered. In order to reduce the number of parameters needed for the simulation of such a complex multilayer, the layers thickness is determined by TEM analysis (see below) while the layer density and interface roughness are the only parameters used to fit the XRR spectra. Particular attention was paid to the density and thickness changes of the Pd, top Fe, MgO and bottom Fe layers and to the Fe/MgO and MgO/Fe interface roughness. Figure 3 shows the changes in the density of the Pd and the two Fe layers. In agreement with the IPROS simulations, it is clear that the upper Fe layer and the Pd one become more

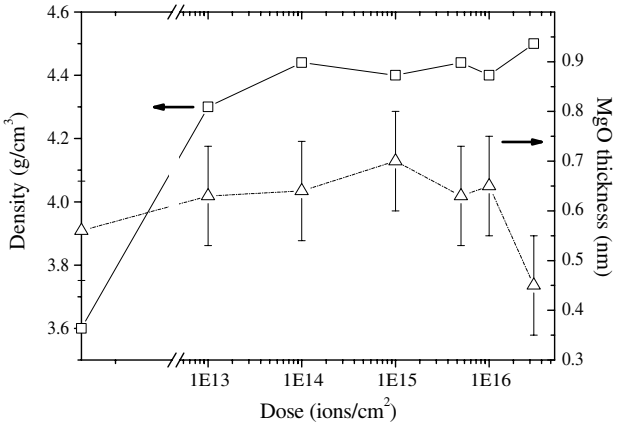

Figure 4. Changes in the density and the thickness of the MgO barrier as a function of the ion dose (the points on the left axis represent the density and thickness of the as-deposited MgO barrier).

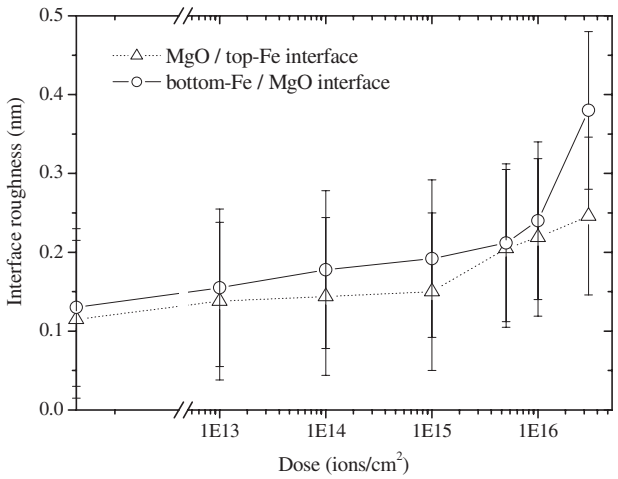

Figure 5. Changes in the MgO/top Fe and bottom Fe/MgO interface roughness as a function of the ion dose (the points on the left axis represent the interfaces roughness of the as-deposited sample).

and more mixed with increasing ion dose, even for doses as low as 10^{14} ions cm^{-2}. For doses higher than 10^{15} ions cm^{-2} the density of the top Fe layer has increased by 30% due to the insertion of Pd (and probably Au) atoms; together the thickness of the top magnetic layer increases from 6.2 nm (as-deposited) to 11 nm (10^{16} ions cm^{-2}). A Pd atom, with an atomic radius of 0.137 nm, cannot stay in the interstitial voids of the Fe-bcc lattice of radius 0.039 nm. Considering only the substitution of Fe by Pd and assuming that the volume of the Fe-bcc unit cell remains constant, we can approximate the content of Pd in the top (Fe, Pd) layer responsible for the increase of the top magnetic layer density. We measure an alloy consisting of about 40% of Pd (this rough calculation does not take into account obvious expansion of the Fe cell, which would, however, give an ever higher Pd content). This content is nevertheless important and should modify the magnetic properties of the top electrode. The density of the bottom Fe layer only slightly increases to a value 12% larger than what would be expected for pure Fe and remains quite constant for doses less than 10^{16} ions cm^{-2} then rises at the highest dose of 3×10^{16} ions cm^{-2}. The content of Pd in the bottom Fe layer can be approximated to 10%.

We reported in figure 4 the modifications of the density and the mean thickness of the MgO barrier. An important increase in the MgO density from 3.6 g cm^{-3} up to 4.3 g cm^{-3} (+22%) is observed when increasing the dose to 10^{13} ions cm^{-2}, it then remains almost constant for higher doses. In the meantime, the MgO thickness continuously increases with dose up to 10^{15} ions cm^{-2} from 0.55 nm to ∼0.7 nm. Assuming the substitution of only Fe ions for Mg (the atomic radius of Fe atoms does not permit them to stay in interstitial position in the MgO lattice) we calculate the percentage of Fe that may be responsible of the MgO density increase and we get 47% of Fe in substitution for Mg in the barrier.

The changes in Fe/MgO/Fe interface roughness as a function of the dose are displayed in figure 5. This indicates a continuous increase of both Fe/MgO and MgO/Fe interface roughness. In the MTJ irradiated at the highest dose (3×10^{16} ions cm^{-2}), the top Fe/MgO roughness abruptly increase to 0.4 nm while the barrier thickness drops to 0.45 nm (figure 4). The accurate XRR simulation of such very rough stacking in which the interface roughness becomes as large as the thickness becomes very difficult. Therefore the results obtained at such a high dose have to be analyzed carefully. However, in agreement with IPROS simulations, when increasing the dose, these XRR measurements indicate a mixing of the top Fe layer with the Pd one with a Pd content as high as 40%. Meanwhile the bottom Fe layer, whose density slightly increases with the dose, is only weakly doped by additional ions (Mg, Fe and/or Pd). At the same time, the Fe/MgO and MgO/Fe interface roughness increases together with the MgO layer density, indicating a doping by Fe (and probably Pd) of the barrier up to 47%.

4.2. Transmission electron microscopy

Figure 6(a) shows a low magnification TEM bright-field image of the as-deposited Au/Pd/Fe(7 nm)/MgO (0.6 nm)/Fe (21 nm) ‖ MgO(001) stacking and a HRTEM micrograph of the Fe/MgO/Fe three-layer is reported in figure 6(b) (with a zoom inset). As already observed in a similar sample [22], the insulating barrier appears to be continuous over a long distance, the epitaxial growth of the whole stacking is confirmed with smooth Fe/MgO and MgO/Fe(001) interfaces. As expected, the MgO barrier is about 0.6 nm thick, corresponding to the stacking of three (002) atomic planes. The quantitative measurement of the (002) interreticular distance in the MgO barrier gives $d_{002} = 0.225$ nm (±0.005 nm) which is slightly larger than the bulk value (0.21 nm). This is in agreement with the expected value for the MgO structure epitaxially strained on Fe(001).

Figures 7(a) and (b) display similar HRTEM micrographs obtained for the MTJs irradiated at doses of 5×10^{15} ion cm^{-2} and 3×10^{16} ions cm^{-2}, respectively. In both HRTEM micrographs, the Pd/Fe interface appears to be much more blurred due to a mixing between both layers in agreement with

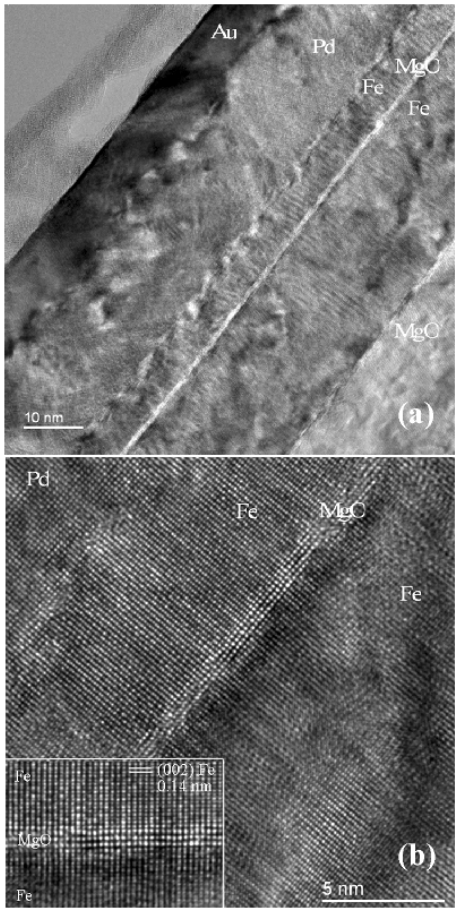

Figure 6. (a) Low magnification TEM image of the as-deposited Au/Pd/Fe/MgO/Fe/MgO(001) MTJ. (b) HREM images of the same stacking. The inset shows a zoom of the Fe/MgO/Fe barrier.

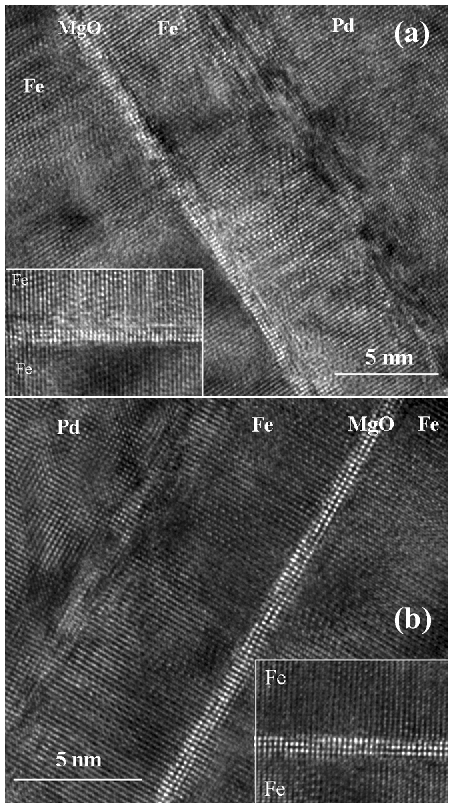

Figure 7. HRTEM micrographs obtained on the MTJ irradiated at doses of (a) 5×10^{15} ion cm^{-2} and (b) 3×10^{16} ions cm^{-2}.

XRR results and IPROS simulations. The MgO barrier is also less perfect, though it remains almost continuous without any evidence of pinholes. Quantitative measurement of the mean MgO lattice parameter does not give evidence of a significant change of the d_{002} interreticular distance compared to what was measured in the as-deposited MTJ. Therefore, we do not expect any relaxation of the strained MgO barrier induced by the ion irradiation.

5. Magnetic measurements

5.1. Holography

Holography results obtained on the as-deposited sample are reported in figures 8(a)–(e). Figure 8(a) is an electron hologram obtained on the whole sample. Figure 8(b) shows the same hologram zoomed in the region of interest. Figures 8(c) and (d) are the phase images corresponding, respectively, to the electrostatic and to the magnetic contributions to the phase shift of the electron beam. They have been calculated after reversing the magnetization as described in the experimental section (see section 2.4). The phase shifts in the electrostatic contribution in figure 8(c) correspond to thickness (t) variations and change in the nature of the layers (V_i) (equation (3)). Assuming a mean inner potential of 17 V for Fe [15], we measure the sample thickness along the beam direction as 30 nm at the center of the image in the area where the top Fe layer stands and 37 nm at the location of the bottom Fe layer. The contrast in the magnetic phase image in figure 8(d) is changing from white to black (red to green in the colored image) in areas where the two Fe layers lie. Note that this intensity is vanishing toward the left part of the phase image where the TEM sample is thinnest in agreement with equation (2). The derivative of equation (2) gives the measurement of the y component of the magnetic induction, i.e. perpendicular to x and z (equation (4)):

$$B_{\perp}(x) = \frac{\hbar}{e \cdot t} \cdot \frac{\mathrm{d}\phi_{\mathrm{Mag}}(x)}{\mathrm{d}(x)}. \tag{4}$$

A quantitative measurement of the remanent magnetization can then be obtained in the two Fe layers from equation (4) using the thickness value deduced from the MIP phase shift (equation (3)). The corresponding image is reported in figure 8(e). In this two opposite contrasts clearly show up on the two Fe layers, indicating that the magnetization in the two Fe layers is anti-parallel while no flux is measured out of these layers. A profile of the magnetic induction along the x direction has been extracted and plotted in figure 9. It clearly shows an inversion in the sign of the magnetic induction in the two Fe layers. This indicates an anti-parallel configuration of the magnetization in the two Fe layers. The magnetization goes to zero where the MgO barrier sets. The mean values for the magnetic remanence in the top and bottom Fe layers were

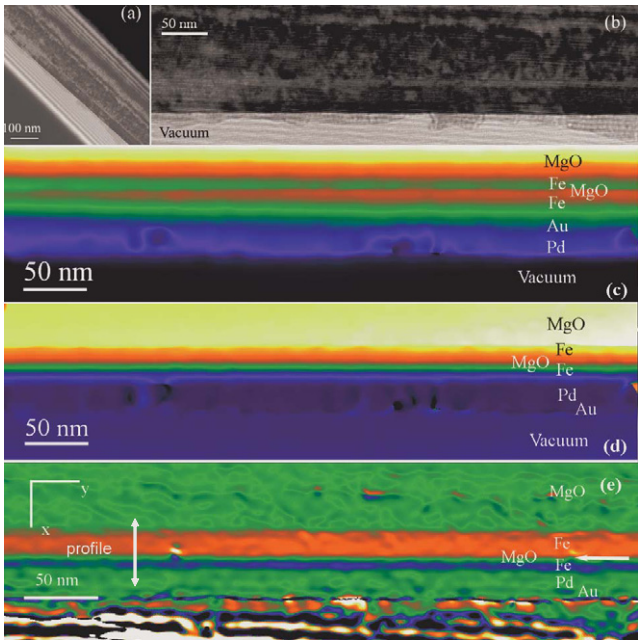

Figure 8. (a) Hologram obtained on the as-deposited MTJs. (b) Zoom of the hologram in the region of interest. (c) Phase image of the electrostatic contribution to the phase shift. (d) Phase image of the magnetic contribution to the phase shift. (e) y component of the local magnetic induction (see text). The antiferromagnetic configuration of the Fe layers separated by the MgO barrier is clearly seen from the color representation (in the electronic version of the journal).

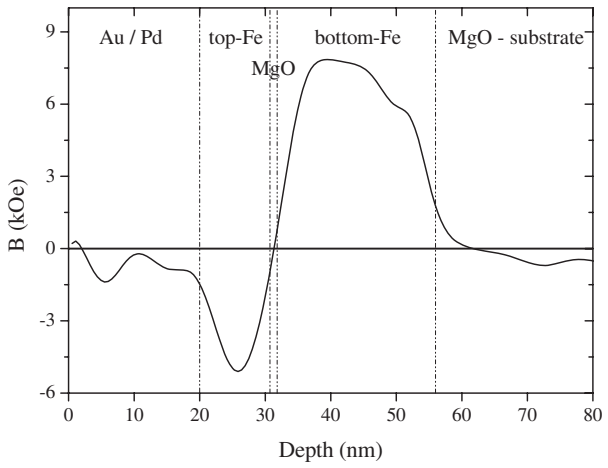

Figure 9. Profile of the magnetic induction across the MTJ integrated along the y direction.

about -4 and 7 kOe, respectively. We assume that the sample prepared for the TEM studies consists of a magnetically active layer whose remanent magnetization is the bulk one ($M_s = 21.6$ kOe) surrounded by two amorphous non-magnetic layers. Thus, we may calculate respectively the thicknesses of the magnetic and non-magnetic layers crossed by the electron beam. We found a ferromagnetic layer of 16 nm inserted between two non-magnetic layers of 10 nm.

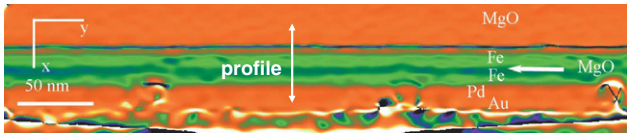

Figure 10. Magnetic induction obtained on the MTJ irradiated at a dose of 3×10^{16} ions cm^{-2}.

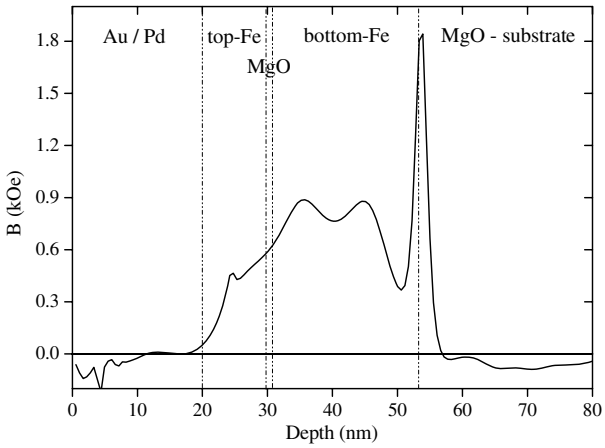

Figure 11. Profile of the magnetic induction across the MTJ irradiated at a dose of 3×10^{16} ions cm^{-2}.

Similar holography experiments were performed on the MTJs irradiated at 5×10^{15} and 3×10^{16} ions cm^{-2}. We show in figure 10 the image of the remanent magnetization obtained by EH on the MTJ irradiated at the highest dose. In this image the two Fe layers are no longer separated. From the colored representation of figure 10 one can directly observe the parallel magnetization configuration of the Fe layers separated by the MgO thin barrier. This configuration depicts a ferromagnetic coupling. The magnetic induction profile plotted along the growth direction (x) in figure 11 reinforced the occurrence of F coupling as both Fe magnetizations are of the same sign.

In the Fe/MgO/Fe samples irradiated at doses of 5×10^{15} ions cm^{-2} we evidenced areas where the Fe layers are AF coupled and other parts of the sample where the configuration of the magnetization is F. Unfortunately we did not succeed experimentally in observing single regions where the IEC switches from AF to F.

We summarize below the EH and structural (TEM and XRR) results obtained on irradiated MTJs:

- The interface roughness (XRR results) is increasing monotonically with the dose.
- In the regime where the holography demonstrates F coupling (dose $\geqslant 5 \times 10^{15}$ ions cm^{-2}), the HRTEM experiments do not demonstrate the presence of pinholes in the MgO barrier (Fe pillars across the MgO layer).
- For such doses, the reflectometry experiments indicate an increase of the density of the barrier related to a large amount of intermixed Fe in the MgO layer.

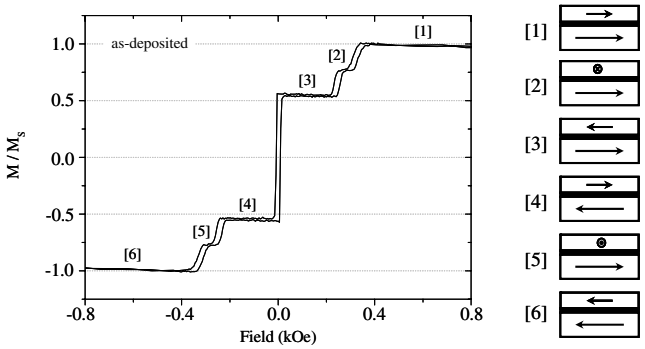

Figure 12. Hysteresis loop of the as-deposited Fe(30 nm)/MgO(0.6 nm)/Fe(10 nm) MTJ with a sketch of the six magnetic configurations ([1]–[6]) of the two Fe layers.

5.2. Vibrating sample magnetometry

Let us first consider the magnetic properties of the as-deposited stack. A typical magnetization curve is presented in figure 12. The field is applied along one of the easy axes of Fe which presents a fourfold anisotropy. At the saturation (state [1]), the Fe layers have their magnetization parallel to the applied field. Reducing the field, the AF coupling tends to stabilize the anti-parallel (AP) configuration. Therefore, during its reversal (state [2]), the magnetization of the thinner layer flips to 90° with respect to the field, being temporarily trapped by the second easy-axis of Fe. In the state [3] the Fe layers are stabilized in the AP configuration, with the net magnetic moment aligned along the positive field. Reversing the applied field in the opposite direction, the net moment switches along the field direction (state [4]) stabilizing again an AP configuration. Increasing the field further, the Fe layers will saturate (state [6]), passing again through the intermediate 90° configuration (state [5]). The AP state of the magnetization in the remanent state has been clearly confirmed by the holography measurements, as shown in the previous section (see figures 8(e) and 9).

The impact of the irradiation on the magnetic behavior is illustrated in figure 13. A qualitative analysis points out immediately the change in the shape of the magnetization loop as the ion irradiation dose increases. For doses from 10^{13} to 10^{15} ions cm^{-2}, the six magnetic states (configurations) measured in a non-irradiated sample remain. However, the values of the saturation field (H_S), the plateau field (H_P) and the 90° field window ($\Delta H_{90°}$) (states [2] and [5]) are strongly influenced by the irradiation, as can be seen in figure 13. For higher doses, above 5×10^{15} ions cm^{-2}, the AF coupling in the magnetization loops disappears. The two Fe layers reverse simultaneously at a coercive field of about 10 Oe. For the highest doses, the VSM measurements therefore confirm the parallel configuration of both Fe magnetizations in the remanent state observed by holography. A more detailed analysis of the impact of the ion dose on the magnetic properties is discussed in the next section.

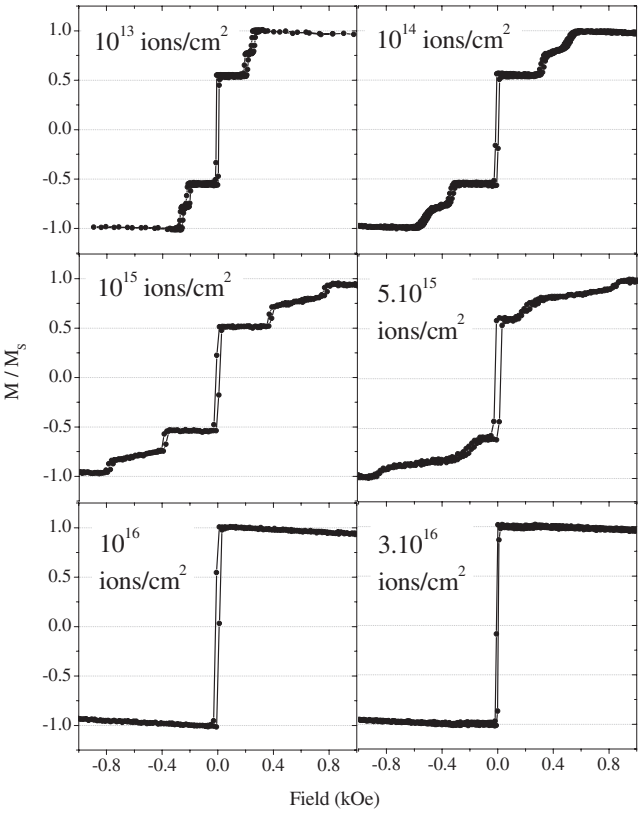

Figure 13. Magnetization loops of the MTJs irradiated at different doses.

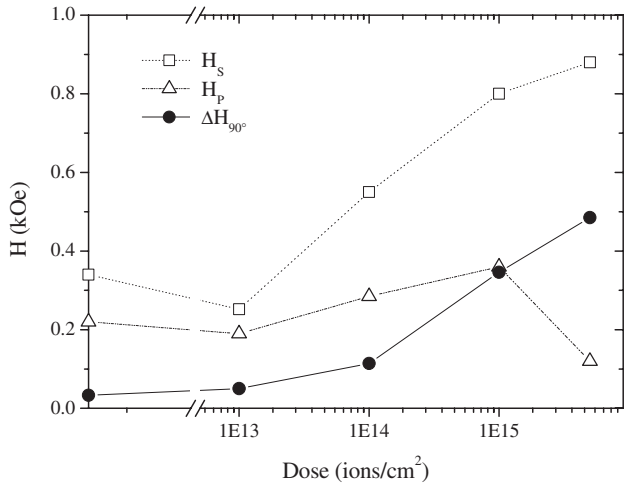

Figure 14. Evolution of the saturation field (H_S), the plateau field (H_P) and the width of the field window for the 90° configuration ($\Delta H_{90°}$) with the irradiation dose (the points on the left axis represent the fields values of the as-deposited sample).

6. Discussion

When the irradiation dose increases from 10^{13} up to 10^{15} ions cm^{-2} the saturation field (H_S) shows a monotonic increase from 270 to 900 Oe as reported in figure 14. Simultaneously, the width of the 90° plateau (H_P), i.e. states [2] and [5] in figure 12, increases from 35 to 500 Oe when the

dose increases to 10^{15} ions cm^{-2}, then decreases. The increase in the plateau field H_P can be explained by an enhancement of the AF bilinear coupling strength J combined with a reduction of the magnetic thickness of the top Fe layer. Following the simple model of coupling by spin tunneling, described by Slonczewski [2], an increase in J could be easily related to a local decrease of the barrier thickness or to a reduction of the wavevector within the barrier. The irradiation affects the structure of the MgO insulator and therefore both events are realistic. Moreover, the reduction of the thickness of the top Fe layer may be explained from the intermixing of the Fe layer with the Pd capping one. These changes are both induced by the ion irradiation as demonstrated by the XRR measurements. The decrease of H_P at doses higher than 10^{15} ions cm^{-2} is directly related to the increase of the width of the field window (ΔH_{90°) corresponding to the intermediate 90° state. It reflects the stability of the 90° configuration (states [2] and [5]) with respect to the 180° one (states [3] and [4]). Moreover, the increase of H_S is correlated with the increase of ΔH_{90°.

As discussed in the introduction, we associate the AF coupling in our samples with the resonant propagation of the interfacial minority spin resonance state of Fe(001) [8]. As reported in [7], the increase in roughness quenches the IRS. We can then extrapolate and argue that the ion irradiation induced roughness of the Fe/MgO interfaces leads to the vanishing of the AF coupling measured in our samples. XRR results indicate that increasing the dose will enhance the interface roughness and the density of the barrier. TEM analyses do not show clear ferromagnetic Fe bridges, but even if the barrier remains continuous a local F coupling is observed from EH experiments. For intermediate doses (5×10^{15} ions cm^{-2}) EH indicates the presence of both F and AF regions. We argue that in the MTJs irradiated at doses up to 5×10^{15} ions cm^{-2} the roughness effect is smaller so that the IEC is only locally destroyed. This superimposition of the F and AF coupling gives rise to a biquadratic coupling whose intensity therefore increases with the irradiation dose. This increase of the biquadratic coupling is reflected by the increase of ΔH_{90° measured in the magnetization loops. It also determines the augmentation of the saturation field H_S: the Zeeman energy has to overcome the increase in the coupling energy.

The occurrence of local F coupling for the high ion dose has been demonstrated by the EH measurements, as previously discussed (figure 10). The XRR measurements show that the larger the ion dose, the larger the Fe/MgO interfacial roughness and the barrier density. This will lead to the final configuration where we experimentally measure a net F coupling in samples where the irradiation dose is higher than 5×10^{15} ion cm^2. In these samples one can assume that the nature of the insulating MgO barrier has been sufficiently modified by intermixing with the two Fe layers to allow direct F coupling between the top and bottom magnetic layers.

Let us now inspect the role of the irradiation on the fourfold anisotropy of the Fe layers. XRR experiments evidence an ion induced intermixing effect at the Pd/Fe interface. This will obviously change the interfacial anisotropy contribution which could affect the total anisotropy of the top Fe layer. However, in the magnetization curves presented in figures 12 and 13 one can notice that the ion dose does not affect either the width of the hysteresis loop corresponding to the magnetization reversal from the saturation to the 90° state or the coercive field of the net moment switch in a negative field. This suggests that the effect of irradiation on the anisotropy can be neglected with respect to the effect on the bilinear and biquadratic coupling.

7. Conclusion

In conclusion, both the macroscopic magnetometry (VSM) and the nanoscopic holographic measurements demonstrate the antiferromagnetic state of the Fe (30 nm)/MgO (0.6 nm)/Fe (10 nm) in zero magnetic field. The amplitude and the type of coupling can be affected by ion irradiation of samples. In non-irradiated samples the coupling is antiferromagnetic with a dominant bilinear term. A gradual increase of the bilinear and biquadratic coupling has been measured when the ion dose increases, with a significant increase of the biquadratic term for larger doses. The biquadratic coupling is explained here by the superposition between antiferromagnetic and ferromagnetic contributions. Finally, for the larger doses used in our experiments, the net coupling becomes purely ferromagnetic, corresponding to a strong structural intermixing of the MgO barrier with the adjacent Fe layers.

A complete description of the irradiation induced effects on the interlayer exchange coupling by spin polarized tunneling in a Fe/MgO/Fe MTJ remains difficult. The first effect is related to the influence of roughness on the interfacial resonant state of the Fe. This affects the amplitude and the sign of the coupling. Following the resonant transport models [5], the quenching of the resonant tunneling mechanism can induce a change of sign (from AF to F) for the coupling mediated by spin tunneling without any need for direct ferromagnetic bridges across the barrier. On the other hand, from the pure tunneling model of Slonczewski [2], a sign reversal of the IEC coupling may be related to the relative amplitude of the wavevector within the barrier and spin dependent wavevector in the ferromagnetic electrodes. Any modification of the barrier properties (i.e. the effect of irradiation) affects the attenuation vector and therefore the amplitude and even the sign of the IEC. The third roughness induced irradiation effect is the direct ferromagnetic coupling across local ferromagnetic bridges created only for large ion doses when we can assume that the insulating barrier is locally 'destroyed'. We mention this last point here, because even if no clear evidence of metallic Fe bridges (i.e. pinholes in the MgO barrier) has been found in our samples one can still wonder about the F coupling mechanism across the 'bridges', mostly constituted by MgO intermixed with Fe atoms. Transport measurements on irradiated MTJs should bring additional information on that point. The last complication arises from the complex transport mechanisms in single crystal Fe/MgO/Fe stacks which should lead to a theoretical background for the IEC coupling beyond the free electron simple models. From a theoretical point of view, this last aspect is still not yet accomplished.

References

[1] Faure-Vincent J, Tiusan C, Bellouard C, Popova E, Hehn M, Montaigne F and Schuhl A 2002 *Phys. Rev. Lett.* **89** 107206

[2] Slonczewski J C 1989 *Phys. Rev.* B **39** 6995

[3] Butler W H, Zhang X G, Schulthess T C and MacLaren J M 2001 *Phys. Rev.* B **63** 054416

[4] Katayama T, Yuasa S, Velev J, Zhuravlev M Ye, Jaswal S S and Tsymbal E Y 2006 *Appl. Phys. Lett.* **89** 112503

[5] Zhuravlev M Ye, Tsymbal E Y and Vedyayev A V 2005 *Phys. Rev. Lett.* **94** 026806

[6] Wunnicke O, Papanikolaou N, Zeller R, Dederichs P H, Drchal V and Kudrnovsky J 2002 *Phys. Rev.* B **65** 064425

[7] Bischoff M M J, Yamada T K, Fang C M, de Groot R A and van Kempen H 2003 *Phys. Rev.* B **68** 045422

[8] Tiusan C, Sicot M, Hehn M, Belouard C, Andrieu S, Montaigne F and Schuhl A 2006 *Appl. Phys. Lett.* **88** 062512

[9] Tiusan C, Sicot M, Faure-Vincent J, Hehn M, Bellouard C, Montaigne F, Andrieu S and Schuhl A 2006 *J. Phys.: Condens. Matter* **18** 941–56

[10] Faye M M, Laanab L, Beauvillain J, Claverie A, Vieu C and Benassayag G 1993 *Two-dimensional Damage Distributions Induced by Localized Ion Implantations* (Pittsburgh, PA: Mater. Res. Soc.)

[11] http://www-llb.cea.fr/prism/programs/simulreflec/simulreflec.html

[12] Snoeck E, Hartel P, Mueller M, Haider M and Tiemeijer P C 2006 *Proc. IMC16 Congr. (Sapporo)*

[13] Midgley P A 2001 *Micron* **32** 167

[14] Rau W D, Schwander P, Baumann F H, Höppner W and Ourmazd A 1999 *Phys. Rev. Lett.* **82** 2614

[15] Twitchett A C, Dunin-Borkowski R E and Midgley P A 2002 *Phys. Rev. Lett.* **88** 238302

[16] Tonomura A 1992 *Adv. Phys.* **41** 59

[17] Dunin Borkowski R E, McCartney M R, Kardynal B, Parkin S S P and Smith D J 2000 *J. Microsc.* **200** 187

[18] Reimer L 1997 *Transmission Electron Microscopy* (Berlin: Springer)

[19] Dunin Borkowski R E, McCartney M R, Smith D J and Parkin S S P 1998 *Ultramicroscopy* **74** 61

[20] Möller W and Eckstein W 1984 *Nucl. Instrum. Methods Phys. Res.* B **2** 814

[21] Möller W, Eckstein W and Biersack J P 1988 *Comput. Phys. Commun.* **51** 355

[22] Popova E, Faure-Vincent J, Tiusan C, Bellouard C, Fischer H, Snoeck E, Hehn M, Montaigne F, Da Costa V, Alnot M, Andrieu S and Schuhl A 2002 *Appl. Phys. Lett.* **81** 1035